J. Fluid Mech. (2018), *vol.* 849, *pp.* 355–372. © Cambridge University Press 2018
doi:10.1017/jfm.2018.451

Flow reversals in two-dimensional thermal convection in tilted cells

Qi Wang[1], Shu-Ning Xia[2], Bo-Fu Wang[2], De-Jun Sun[1], Quan Zhou[2] and Zhen-Hua Wan[1,†]

[1]Department of Modern Mechanics, University of Science and Technology of China, Hefei 230027, China

[2]Shanghai Institute of Applied Mathematics and Mechanics, Shanghai University, Shanghai 200072, China

(Received 9 February 2018; revised 23 April 2018; accepted 24 May 2018; first published online 18 June 2018)

The influence of tilt on flow reversals in two-dimensional thermal convection in rectangular cells with two typical aspect ratios, Γ = width/height = 1 and 2, are investigated by means of direct numerical simulations. For $\Gamma = 1$, tilt tends to suppress flow reversals. However, it is found that flow reversals characterized by two main rolls are promoted by tilt for $\Gamma = 2$, which are even observed for some cases of small Prandtl numbers (Pr) and large tilt angles (β). Different from level cases where the four corner rolls all have opportunities to grow and trigger a flow reversal, the reversals in an anticlockwise tilted cell with $\Gamma = 2$ are always led by the growth of the bottom-right or the top-left corner roll. Tilt is favourable for the growth of the bottom-right or the top-left corner roll and thus for breaking the balance between the two main rolls and triggering a flow reversal. The mode decomposition analysis shows that the appearance of the intermediate single-roll mode is crucial for reversals, and flow reversals in a tilted cell with $\Gamma = 2$ can be viewed as a mode competition process between single-roll mode and horizontally adjacent double-roll mode. They can only occur in a limited range of β where the two modes have comparable strength. Furthermore, the Nusselt numbers at the hot plate Nu_h and at the cold plate Nu_c behave differently during a flow reversal for $\Gamma = 2$ due to the preference of single corner roll growth.

Key words: Bénard convection, convection, convection in cavities

1. Introduction

Spontaneous reversal phenomena are common in many buoyancy-driven fluid dynamical systems, including reversals of the Earth's geomagnetic field (Glatzmaier & Roberts 1995), and large-scale fluid motion in the sea and the atmosphere (van Doorn *et al.* 2000). There also exist flow reversals of the large-scale circulation (LSC) in a model problem, i.e. Rayleigh–Bénard convection (RBC) where a fluid layer is heated from below and cooled from above (see Ahlers, Grossmann & Lohse 2009; Xia 2013; Verma, Kumar & Pandey 2017, and references therein). The study of flow

† Email address for correspondence: wanzh@ustc.edu.cn

https://doi.org/10.1017/jfm.2018.451 Published online by Cambridge University Press

reversals in a model system like RBC may enable us to gain more insights into general reversal phenomena in nature (Huang *et al.* 2015).

In cylindrical cells, there are two categories of flow reversals (Brown, Nikolaenko & Ahlers 2005): one is rotation-led reversals, which are caused by incessant azimuthal meandering of the circulating plane; the other is cessation-led reversals, in which the LSC slows to a stop and restarts in a random new orientation. Flow reversals in cylindrical cells have been studied both experimentally (Brown *et al.* 2005; Brown & Ahlers 2006; Xi, Zhou & Xia 2006; Xi & Xia 2007, 2008*a*,*b*; Xi *et al.* 2016) and numerically (Mishra *et al.* 2011). Several models, either stochastic ones (Benzi 2005; Brown & Ahlers 2007) or deterministic ones (Araujo, Grossmann & Lohse 2005), have been proposed to account for the flow reversals. The model proposed by Brown & Ahlers (2007) consists of two stochastic ordinary differential equations, and it agrees well with many experimental results for LSC dynamics. The recent experimental work of Xi *et al.* (2016) found that the second mode and the remaining higher-order modes play important roles in the dynamical process of the reversal and the Nusselt number Nu drops to its minimum during a flow reversal. It was once thought that cessation-led reversals presumably would prevail in systems where the rotational invariance is broken (Brown *et al.* 2005). However, the cessations of the LSC have not been observed in a cubic cell where the rotational invariance is broken (Foroozani *et al.* 2017). It is still ambiguous why cessations are absent in a cubic cell.

Without complicated three-dimensional (3D) structures, flow reversals in two-dimensional (2D) (Sugiyama *et al.* 2010; Chandra & Verma 2011, 2013; Petschel *et al.* 2011; Podvin & Sergent 2015; Verma, Ambhire & Pandey 2015; Castillo-Castellanos, Sergent & Rossi 2016; Xia *et al.* 2016; Mannattil *et al.* 2017; Podvin & Sergent 2017) or quasi-2D (Huang *et al.* 2015; Ni, Huang & Xia 2015; Huang & Xia 2016) square cavities have attracted much attention in recent years. Sugiyama *et al.* (2010) studied flow reversals in a square cavity with unit aspect ratio by means of 2D direct numerical simulations (DNS) combined with experiments performed in a quasi-2D cell, and found that the results of experiments and simulations are in very good agreement. They also showed that the growth of corner rolls both in kinetic energy and in size plays key roles in triggering flow reversals. They concluded that flow reversals in a 2D/quasi-2D cell occur only in a limited parameter space, that is to say, the reversals do not exist for too large or too small Pr as well as too large or too small Ra. Chandra & Verma (2011, 2013) used a mode decomposition method to study flow reversals, and showed that flow reversals are caused by a vortex reconnection of two attracting rolls and the appearance of the (2, 2) mode is critical to trigger flow reversals. Podvin & Sergent (2015, 2017) used proper orthogonal decomposition to study flow reversals in a 2D square cell and proposed a 3D model that is based on the interaction of the LSC, the quadrupolar flow and horizontal rolls. Castillo-Castellanos *et al.* (2016) found that the reversal cycle is composed of three successive phases: acceleration, accumulation and release including a rebound event. Huang & Xia (2016) experimentally found that the frequency of flow reversals increases drastically in smaller Γ cells. It should be noted that 2D/quasi-2D convection promotes reversals particularly for topological reasons. In 3D cubic cells, reversals are very rare (Foroozani *et al.* 2017). Previous works are almost restricted to a unit-aspect-ratio cell where there exists only one LSC that spans the size of the convection cell. It has already been realized by Sugiyama *et al.* (2010) that Γ has a strong effect on the reversal dynamics. For a $\Gamma = 2$ cell, the flow is characterized by two main rolls and flow reversals also exist (Chandra & Verma 2011; Verma *et al.* 2015). However, much less work has so far been devoted to flow reversals in a $\Gamma = 2$ cell.

https://doi.org/10.1017/jfm.2018.451 Published online by Cambridge University Press

There are several differences between flow reversals in 2D/quasi-2D and 3D geometries. Firstly, the mean time between successive reversals has a strong *Ra* dependence in the former (Sugiyama *et al.* 2010) while it has a weak *Ra* dependence in the latter (Brown & Ahlers 2006; Xi & Xia 2007). Secondly, flow reversals in 2D/quasi-2D cells occur in a limited parameter space, and there are no reversals for *Ra* larger than 5×10^8 (2D) or 1.6×10^9 (quasi-2D) (Sugiyama *et al.* 2010). However, flow reversals in 3D cylindrical cells can occur at larger *Ra* ($Ra > 10^{10}$) (Brown *et al.* 2005; Brown & Ahlers 2006; Xi *et al.* 2016) and high *Pr* ($Pr = 19.4$) (Xie, Wei & Xia 2013). Whether 2D reversals and cessation-led reversals correspond to the same phenomenon is still an open question (Castillo-Castellanos *et al.* 2016).

Almost all previous studies are conducted in a symmetrical system. However, flow reversals in the real world usually take place in an asymmetrical system. One example is that the heat flux on the core–mantle boundary in the Earth is non-uniform (Gubbins *et al.* 2011) and this has a great influence on the frequency of geomagnetic reversals (Glatzmaier *et al.* 1999). Another is the solar convection zone that has both torsional oscillations and periodic reversals (Howard & LaBonte 1980). Therefore, it is important to study the influence of symmetry breaking on flow reversals. Brown & Ahlers (2006, 2008) found that flow reversals in a $\Gamma = 1$ cylindrical container are suppressed significantly even for very small tilt angles. Sun, Xi & Xia (2005) also found that, in a cylindrical container with $\Gamma = 0.5$, a minor tilt of 2° will lock the LSC in the azimuthal plane along the tilted direction, and reversals are suppressed; similar results were also found in a rectangular cell with $\Gamma = 0.5$ (Wang *et al.* 2017). Xia *et al.* (2016) studied non-Oberbeck-Boussinesq (NOB) effects on flow reversals, and, interestingly, they found that, when considering NOB effects, flow reversals can be observed for relatively small $Pr = 0.71$. Huang *et al.* (2015) studied the influence of thermal boundary conditions on flow reversals. They claimed that the reversal of the LSC can be viewed as a process for the system to restore its symmetry in a statistical way.

It is generally accepted that tilt will suppress flow reversals in a $\Gamma = 1$ cell. However, how cell tilt will influence flow reversals in larger-aspect-ratio cells where multiple convection rolls may exist is still an open question. In this paper, we try to fill this gap by studying the influence of cell tilt on flow reversals in a 2D rectangular cell with $\Gamma = 2$ where two convection rolls may develop; the results are also compared with those for $\Gamma = 1$ cases. The reason why we choose $\Gamma = 2$ is that it has been found previously that flow reversals of a double-roll state exist in a $\Gamma = 2$ cell (Chandra & Verma 2011; Verma *et al.* 2015), while whether flow reversals exist for $\Gamma > 2$ is still unknown. There are two advantages of 2D DNS: (i) The numerical effort required for 2D simulations is much smaller and thus we can study flow reversals in a considerable fraction of the Rayleigh number *Ra*/Prandtl number *Pr* versus tilt angle β parameter space for different Γ. (ii) The flow visualization is much easier, and a detailed flow reversal scenario can be obtained. In recent years, 2D DNS has been used widely to study turbulent convection. For example, it has been used to study turbulent heat transfer (van der Poel, Stevens & Lohse 2011; van der Poel *et al.* 2012, 2014; Huang & Zhou 2013; Bao *et al.* 2015), to study boundary layer (BL) dynamics (Zhou *et al.* 2010, 2011; van der Poel *et al.* 2015; Zhang *et al.* 2017*a*), to reveal NOB effects on flow organization (Sugiyama *et al.* 2009), to probe the effect of roughness on heat transfer (Shishkina & Wagner 2011; Toppaladoddi, Succi & Wettlaufer 2017; Zhu *et al.* 2017; Xu *et al.* 2018; Zhang *et al.* 2018), to investigate statistics of kinetic and thermal energy dissipation rates in RBC (Zhang, Zhou & Sun 2017*b*) and, more recently, to explore the transition to the ultimate regime (Zhu *et al.* 2018).

https://doi.org/10.1017/jfm.2018.451 Published online by Cambridge University Press

The remainder of the paper is organized as follows. In § 2, we introduce the governing equations and numerical methods. The main results are presented in § 3, which is divided into three parts. Section 3.1 studies the influence of tilt on flow reversals in $\Gamma = 1$ and $\Gamma = 2$ cells. In § 3.2, we use a mode decomposition method to reveal the inherent mechanism for the reversals in a tilted $\Gamma = 2$ cell. Section 3.3 discusses the heat transfer properties during the reversals. Finally, a short summary is presented in § 4.

2. Numerical procedures

We studied flow reversals in a tilted cell with width $\hat{W}$ and height $\hat{H}$ (hatted quantities are dimensional), where the bottom plate has a constant high temperature $\hat{T}_H$ while the top plate has a constant low temperature $\hat{T}_C$. Here, with Oberbeck–Boussinesq approximation, the dimensionless governing equations read

$$\boldsymbol{\nabla} \cdot \boldsymbol{u} = 0, \tag{2.1}$$

$$\frac{\partial \boldsymbol{u}}{\partial t} + \boldsymbol{u} \cdot \boldsymbol{\nabla} \boldsymbol{u} = -\boldsymbol{\nabla} p + \sqrt{\frac{Pr}{Ra}} \nabla^2 \boldsymbol{u} + T\boldsymbol{e}, \tag{2.2}$$

$$\frac{\partial T}{\partial t} + \boldsymbol{u} \cdot \boldsymbol{\nabla} T = \frac{1}{\sqrt{Ra\,Pr}} \nabla^2 T, \tag{2.3}$$

where $\boldsymbol{u} = (v, w)$ and $\boldsymbol{x} = (y, z)$ are the velocity components and coordinates in the horizontal and vertical directions, p is the reduced kinetic pressure, T is the temperature, $\boldsymbol{e}$ is a unit vector defined by $\boldsymbol{e} = (\sin(\beta), \cos(\beta))$, and β is the tilt angle, which is positive when the cell rotates anticlockwise. For non-dimensionalization, the free-fall velocity $\hat{U} = (\hat{g}\hat{\alpha}\Delta\hat{T}\hat{H})^{1/2}$ and the height of the container $\hat{H}$ are used, where $\hat{g}$ is the gravitational acceleration, $\hat{\alpha}$ is the isobaric thermal expansion coefficient, and $\Delta\hat{T} = \hat{T}_H - \hat{T}_C$ is the temperature difference. The reference time is the free-fall time $\hat{t}_f = \hat{H}/\hat{U}$, and the dimensionless temperature is defined by $T = (\hat{T} - \hat{T}_C)/\Delta\hat{T}$. This problem is governed by three dimensionless parameters, i.e. the Prandtl number Pr, Rayleigh number Ra and aspect ratio Γ:

$$Pr = \frac{\hat{\nu}}{\hat{\kappa}}, \quad Ra = \frac{\hat{g}\hat{\alpha}\Delta\hat{T}\hat{H}^3}{\hat{\nu}\hat{\kappa}}, \quad \Gamma = \frac{\hat{W}}{\hat{H}}, \tag{2.4a–c}$$

where $\hat{\kappa}$ is the thermal diffusivity, and $\hat{\nu}$ is the kinematic viscosity. No-slip and impermeability conditions are imposed at all walls and the sidewalls are insulated.

The governing equations are solved numerically by a well-validated in-house code lMn2d. All spatial terms are discretized using a second-order central difference scheme. A non-uniform grid with clustered grid points near walls is used to resolve small scales inside boundary layers. Pressure and velocities are staggered in space in order to avoid pressure–velocity decoupling. Time integration is accomplished by using the Adams–Bashforth scheme for the nonlinear terms and the Crank–Nicolson scheme for the viscous and diffusion terms. Detailed numerical schemes and validations of this code can be found in our previous work (Xia *et al.* 2016).

The simulation parameters of this paper are listed in table 1. The initial field for cases with $\beta = 0^\circ$ is the conductive state with small perturbations added to the temperature field, while for tilted cases we use the flow field of $\beta = 0^\circ$ as the initial condition. In all cases, the simulations run for a long time to determine whether flow reversals exist. Moreover, in order to obtain better statistics of the flow reversal frequencies, the longest simulation is performed for 249 000 free-fall time units.

https://doi.org/10.1017/jfm.2018.451 Published online by Cambridge University Press

Γ	Ra	Pr	β (deg.)	$N_y \times N_z$
1	$[10^7, 10^8]$	2	[0, 20]	256×256
1	5×10^7	[1.5, 5]	[0, 20]	256×256
2	10^7	[0.05, 4.38]	[0, 90]	512×256
2	$[10^7, 10^8]$	0.3	[0, 60]	512×256

TABLE 1. Simulation parameters. The columns from left to right indicate aspect ratio, Rayleigh number, Prandtl number, tilt angle and mesh resolution.

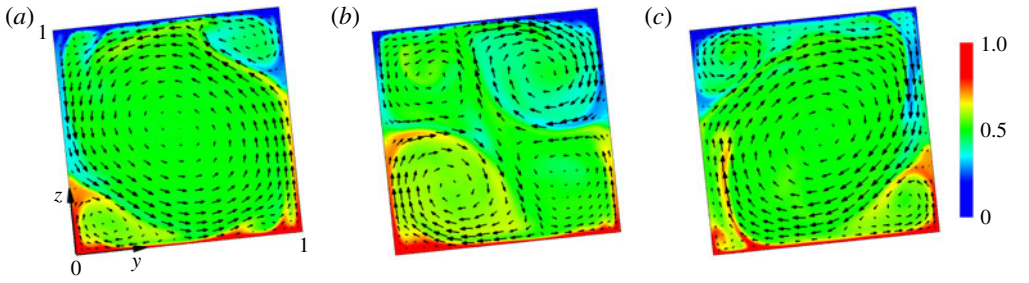


FIGURE 1. (Colour online) Three snapshots of the temperature field superimposed with velocity vectors during one of the flow reversals for $Ra = 5 \times 10^7$, $Pr = 2$, $\beta = 6°$ at different times: (*a*) $t = 500$, (*b*) $t = 655$ and (*c*) $t = 705$.

3. Results and discussion

3.1. *Flow reversals in two-dimensional tilted cells*

We start by studying the influence of tilt on flow reversals for a typical aspect ratio $\Gamma = 1$. Figure 1 shows snapshots of the temperature and velocity fields during one of the reversals at $Ra = 5 \times 10^7$, $Pr = 2$ and $\beta = 6°$. Although the symmetry of the system is broken, it is found that the reversal process is similar to the level case (Sugiyama *et al.* 2010). The two corner rolls grow simultaneously in kinetic energy and also in size due to the plume detachment from the boundary layers, until they merge as a new LSC with the opposite direction, and a flow reversal happens. It is well known that flow reversals occur in a certain Ra–Pr parameter space for $\Gamma = 1$. For a system with only one main roll, the reversal process can be nicely indicated by a global quantity, i.e. the net angular momentum

$$L(t) = \langle -(z - 1/2)v(\boldsymbol{x}, t) + (y - 1/2)w(\boldsymbol{x}, t)\rangle_V, \tag{3.1}$$

where $\langle\cdot\rangle_V$ represents averaging over the total area. Figure 2 shows the time evolution of L for the level case with $\beta = 0°$ and the tilted case with $\beta = 6°$ at $Ra = 5 \times 10^7$ and $Pr = 2$. A sign change of L can reveal a reversal; frequent flow reversals in a level cell can be observed in figure 2(*a*). From figure 2(*b*), it is evident that the symmetry breaking induced by tilt greatly suppresses flow reversals for $\Gamma = 1$. One sees that the clockwise main roll with negative L stays for quite a short time before reversing its orientation. This is because, for the clockwise LSC, as shown in figure 1(*c*), tilt introduces a horizontal buoyancy force along the y direction so that the hot plumes are more likely to move up to the bottom-right corner roll and the cold plumes tend to move down to the top-left corner roll. The two corner rolls have more opportunities

https://doi.org/10.1017/jfm.2018.451 Published online by Cambridge University Press

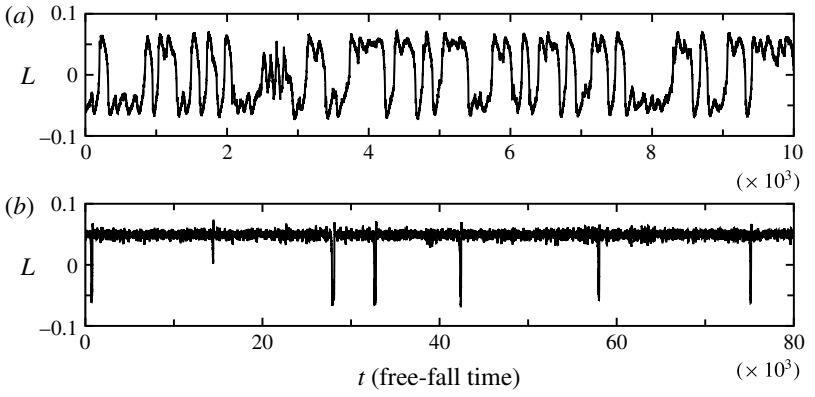


FIGURE 2. Time evolution of the angular momentum L for $\Gamma = 1$, $Ra = 5 \times 10^7$ and $Pr = 2$: (*a*) $\beta = 0°$ and (*b*) $\beta = 6°$. The positive and negative signs indicate anticlockwise and clockwise circulations, respectively.

to grow and trigger a reversal. Besides, the tilt may weaken the clockwise LSC since along the hot and cold plates the horizontal buoyancy force is in the opposite direction to the flow velocity of LSC. Thus the clockwise LSC is less stable and is easier to reverse its orientation, and it always stays for a much shorter time as shown in figure 2(*b*). Previous studies have shown that the main roll will be locked in the plane along the tilted direction both in cylindrical cells (Xi, Lam & Xia 2004; Brown & Ahlers 2006; Shishkina & Horn 2016) and in rectangular cells (Guo *et al.* 2015, 2017) with $\Gamma = 1$. Thus the suppression of flow reversals by tilt for $\Gamma = 1$ is within expectation.

We then map out phase diagrams for $\Gamma = 1$ over β–Pr parameter space with $Ra = 5 \times 10^7$ and over β–Ra parameter space with $Pr = 2$ in figure 3. We run for at least 5000 large-eddy turnover times t_E to detect whether flow reversals exist. Time t_E is defined by $t_E := 4\pi/\langle|\omega_c(t)|\rangle$, where ω_c denotes vorticity in the centre of the main roll. For some cases (for example, $Ra = 10^8$, $Pr = 2$, $\Gamma = 1$, $\beta = 3°$), we even calculate for more than $10\,000\,t_E$ to conclude there are indeed no reversals. As shown in figure 3(*a*), the critical angle β_c displays a non-monotonic relation with Pr. For larger Pr, the β_c value is smaller; for $Pr = 5$, a minor tilt of 1° will completely suppress flow reversals due to the fact that the thickness of the thermal BL is much smaller than the thickness of the kinetic BL and thermal coupling between the corner roll and the thermal BL is weakened, as stated previously (Sugiyama *et al.* 2010). For small Pr, thermal diffusion becomes dominant and suppresses the growth of the corner roll. Therefore, flow reversals in the tilted cell also occur more easily at intermediate Pr, and the corresponding β_c is also larger. In figure 3(*b*), β_c also displays a non-monotonic relation with Ra. For intermediate Ra, the corresponding β_c is larger. The reason lies in the non-monotonic dependence of the flow reversal frequency on Ra. It can be seen in figure 3 of Sugiyama *et al.* (2010) that flow reversals are most frequent for intermediate Ra (approximately 7×10^7 for $Pr = 4.3$); any increase or decrease of Ra will reduce the flow reversal frequency. For the $Pr = 2$ considered in our work, the reversals are most frequent for $Ra \sim 4 \times 10^7$, thus the corresponding β_c is larger, and any increase or decrease of Ra will reduce β_c. The reversals occur less and less frequently with increasing Ra and reversals disappear when $Ra \geqslant 2 \times 10^8$ for $Pr = 2$ (Sugiyama *et al.* 2010). Thus the main roll here is more sensitive to tilt at larger Ra, and a minor tilt of the cell will suppress flow reversals at relatively high Ra.

https://doi.org/10.1017/jfm.2018.451 Published online by Cambridge University Press

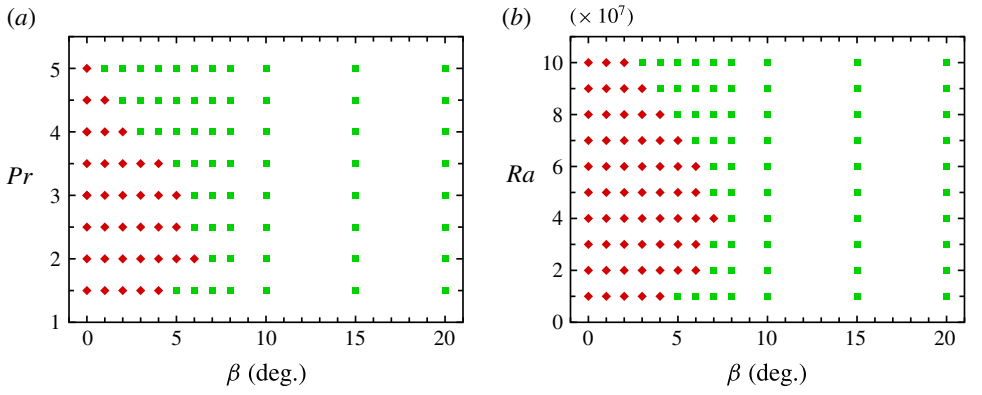


FIGURE 3. (Colour online) (*a*) Phase diagram in the β–Pr plane for $Ra = 5 \times 10^7$, $\Gamma = 1$. (*b*) Phase diagram in the β–Ra plane for $Pr = 2$, $\Gamma = 1$. Red filled diamonds (◆) correspond to detected flow reversals, and green squares (■) to a single-roll state without reversals.

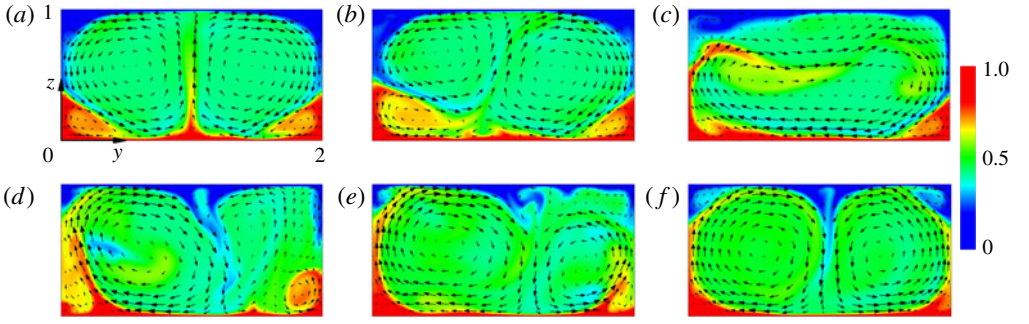


FIGURE 4. (Colour online) Six snapshots of the temperature field superimposed with velocity vectors during one of the flow reversals for $Ra = 10^7$, $Pr = 0.71$, $\beta = 0°$ at different times: (*a*) $t = 12\,283$, (*b*) $t = 12\,338$, (*c*) $t = 12\,349$, (*d*) $t = 12\,354$, (*e*) $t = 12\,361$ and (*f*) $t = 12\,377$.

Compared with $\Gamma = 1$, there have been fewer studies devoted to horizontally adjacent double-roll reversals in a $\Gamma = 2$ cell (Chandra & Verma 2011; Verma *et al.* 2015). Here, we first explore the flow reversals in a $\Gamma = 2$ cell at a fixed $Ra = 10^7$, but varying Pr and β, as listed in table 1. The Ra dependence for a fixed $Pr = 0.3$ is also studied. Figure 4 shows flow reversal scenarios for a level case with $Ra = 10^7$, $Pr = 0.71$ and $\Gamma = 2$; it is seen that the single corner roll growth leads to a flow reversal, which is qualitatively the same as that of Verma *et al.* (2015). Owing to the inherent symmetry of the system, the two bottom corner rolls in figure 4(*a*) and the two top corner rolls in figure 4(*f*) all have opportunities to grow and trigger flow reversals. However, when the symmetry of the system is broken by tilt, the two corner rolls will no longer play equivalent roles.

Figure 5 shows snapshots for two successive flow reversals at $Ra = 10^7$, $Pr = 0.71$ and $\beta = 1°$. As shown in figure 5(*a*), the flow field is characterized by two main rolls and two bottom corner rolls. Since tilt will introduce a horizontal buoyancy force along the y direction, the hot plumes detached from the lower BL will bear

https://doi.org/10.1017/jfm.2018.451 Published online by Cambridge University Press

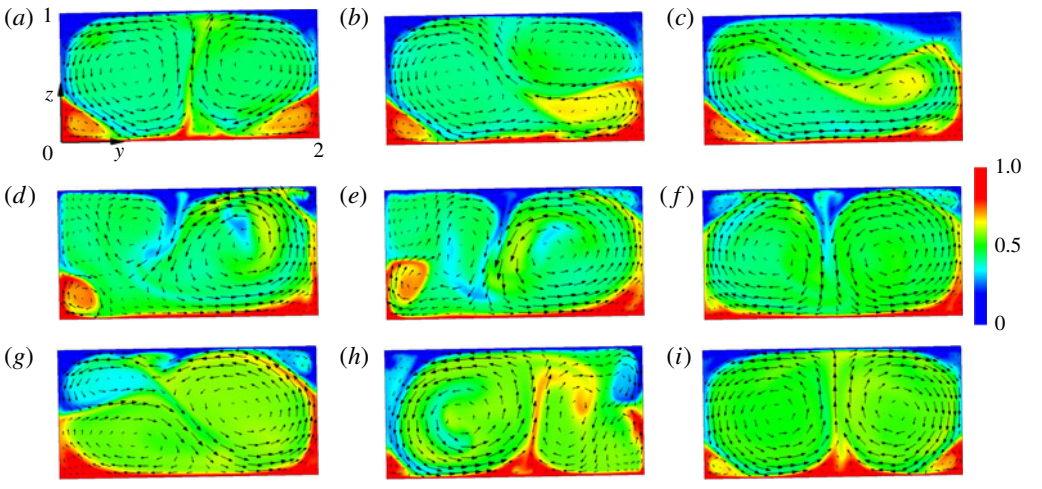


FIGURE 5. (Colour online) Nine snapshots of the temperature field superimposed with velocity vectors during two of the flow reversals for $Ra = 10^7$, $Pr = 0.71$, $\beta = 1^\circ$ at different times: (*a*) $t = 1684.5$, (*b*) $t = 1701$, (*c*) $t = 1704$, (*d*) $t = 1710$, (*e*) $t = 1711.5$, (*f*) $t = 1725$, (*g*) $t = 2860.5$, (*h*) $t = 2869.5$ and (*i*) $t = 2890.5$.

a top-right buoyancy force and be apt to feed the bottom-right corner roll. This is favourable for the growth of the bottom-right corner roll as illustrated in figure 5(*b*). The bottom-left corner roll, however, almost remains unchanged. The subsequent reversal process shown in figure 5(*c–f*) is similar to that in a level case. Similarly, for the next reversal cycle, due to the y direction buoyancy force introduced by tilting the cell, the cold plumes detached from the upper BL are more likely to enter the top-left corner roll. Thus the top-left corner roll growth will lead to a flow reversal, as shown in figure 5(*g–i*). It should also be noted that the horizontal buoyancy force induced by tilt near the top and bottom walls is always in the opposite direction to the flow velocity of one of the two main rolls. Thus the effect of tilt on the main rolls may always play some roles in flow reversals in a tilted $\Gamma = 2$ cell, and the unstable clockwise main roll will always first reverse its direction. Owing to the symmetry breaking, only the bottom-right corner roll in figure 5(*a*) and the top-left corner roll in figure 5(*f*) have opportunities to grow and lead to a flow reversal; this is different from a level case where the four corner rolls all have opportunities to grow and trigger a flow reversal. This argument can be quantitatively demonstrated by investigating the long-time evolution of L as shown in figure 6. Note that L is calculated with respect to the centre point (1, 0.5) here. The flow is dominated by the double-roll mode with $L \simeq 0$ most of the time due to compensation of two main rolls. When flow reversal occurs, the clockwise/anticlockwise intermediate single-roll mode appears (see figures 4*c* and 5*c*), and thus large negative/positive L will appear, indicated by sharp spikes in figure 6. The large positive L indicates that it is the growth of the bottom-right corner roll shown in figure 5(*a*) or the top-left corner roll shown in figure 5(*f*) that leads to flow reversals, while the large negative L indicates that it is the growth of the bottom-left corner roll shown in figure 4(*a*) or the top-right corner roll shown in figure 4(*f*) that leads to a successful flow reversal. It is seen that both positive and negative spikes exist for the level case while only positive spikes exist for the tilted case. Thus only the growth of the bottom-right

https://doi.org/10.1017/jfm.2018.451 Published online by Cambridge University Press

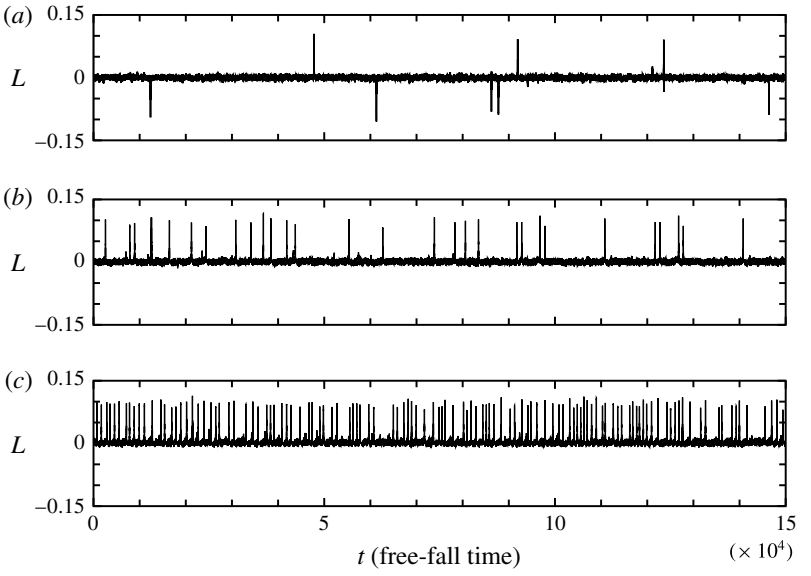


FIGURE 6. Time evolution of angular momentum L for $Ra = 10^7$, $Pr = 0.71$ and $\Gamma = 2$: (*a*) $\beta = 0°$, (*b*) $\beta = 0.5°$ and (*c*) $\beta = 1°$.

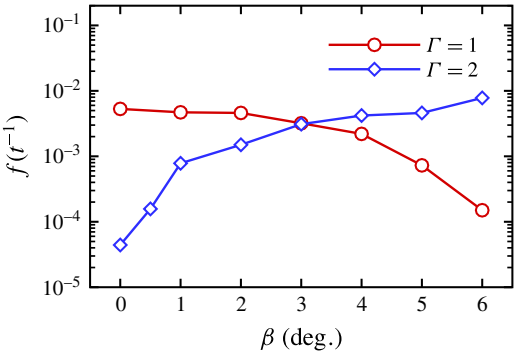


FIGURE 7. (Colour online) Flow reversal frequency f as a function of β. Red circles (○) for $Ra = 5 \times 10^7$, $Pr = 2$, $\Gamma = 1$; blue diamonds (◇) for $Ra = 10^7$, $Pr = 0.71$, $\Gamma = 2$.

corner roll or the top-left corner roll will lead to a flow reversal in a tilted cell. From figure 6, we can also see that there are many more flow reversals in tilted cells, demonstrating that tilt will promote flow reversals for $\Gamma = 2$. To further quantify the promoting effect of cell tilt on the flow reversal, the reversal frequencies f defined by reversal numbers per free-fall time unit are calculated, which are plotted in figure 7. Clearly, for $\Gamma = 1$, f does not drop much for small $\beta \leqslant 2°$, while for $\beta > 2°$, f drops rapidly. In contrast, f increases monotonically with β for $\Gamma = 2$; it even increases more than an order from $\beta = 0°$ to $1°$. Thus a minor tilt will greatly promote flow reversals for $\Gamma = 2$.

Again we map out flow states in β–Pr space for $Ra = 10^7$ and $\Gamma = 2$ in figure 8(*a*). We run for at least $4000\,t_E$ to detect whether flow reversals exist. As the position of the centre of the main roll changes after reversals (this is especially evident for

https://doi.org/10.1017/jfm.2018.451 Published online by Cambridge University Press

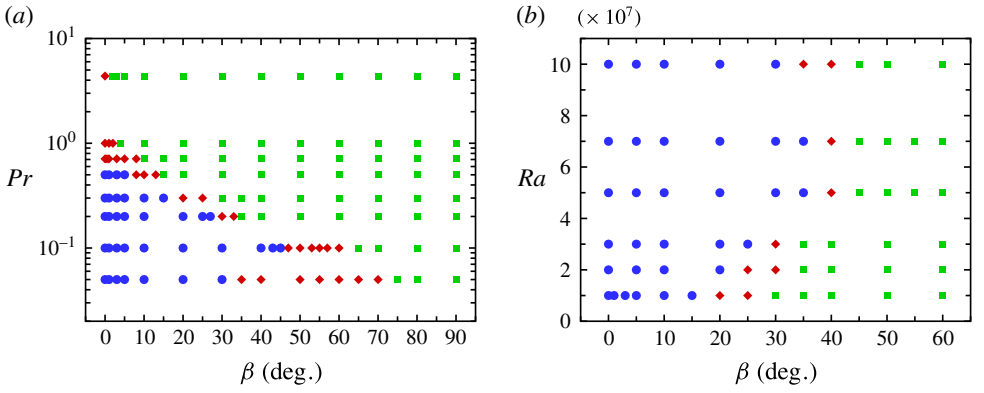


FIGURE 8. (Colour online) (*a*) Phase diagram in the β–Pr plane for $Ra = 10^7$, $\Gamma = 2$. (*b*) Phase diagram in the β–Ra plane for $Pr = 0.3$, $\Gamma = 2$. Red filled diamonds (◆) correspond to detected flow reversals; blue filled circles (●) denote double-roll state without flow reversals; green squares (■) represent single-roll state without flow reversals.

reversals with large β), the large-eddy turnover time t_E is better defined by $t_E := (W + 2H)/u_{LSC}$, where u_{LSC} is the typical velocity of the LSC measured at $\sim H/10$ from the sidewalls and plates (Zhou *et al.* 2011; Ni *et al.* 2015). Three different flow states are identified, which are the double-roll state without flow reversals, the double-roll state with flow reversals, and the single-roll state without flow reversals, respectively. One sees that, for $Pr \leqslant 0.5$ and small β, the flow stays in the stable double-roll state without flow reversals. When β is beyond a critical value, the double-roll state is no longer stable and flow reversals occur in the intermediate range of β. However, when β increases further, the flow becomes a stable one-roll state and no reversals can be observed any more. For $0.71 \leqslant Pr \leqslant 4.38$, the flow transits directly from reversal state to one-roll state. It is interesting that for relatively small $Pr \leqslant 0.5$, flow reversals can only occur in tilted cells. It is worth mentioning that the reversals even occur at very small Pr and large β. For instance, there exist flow reversals for $Pr = 0.05$ and $\beta = 70°$, as seen in figure 8(*a*). This is in stark contrast to that in a $\Gamma = 1$ cell where no reversals exist for $Pr \leqslant 0.71$ (Sugiyama *et al.* 2010). Because flow reversals in tilted cells with $\Gamma = 2$ tend to occur for small Pr, the Ra dependence of flow reversals is studied for a representative small $Pr = 0.3$. Figure 8(*b*) maps out flow states over the β–Ra parameter space for fixed $Pr = 0.3$. It is obvious that flow reversals can only be found in tilted cells, which even exist at $Ra = 10^8$. Based on the above findings, we show that the symmetry breaking of the system induced by tilt has considerably broadened the original Ra–Pr parameter space of flow reversals for $\Gamma = 2$. However, the crucial question left in this section is why reversals only occur in a limited range of β for $\Gamma = 2$.

3.2. *Mode decomposition analysis*

To find the answer to the question left in § 3.1, a mode decomposition method is employed. We project the velocity components v and w onto the following Fourier basis:

$$\hat{v}^{m,n} = \sqrt{2}\sin(m\pi y/2)\cos(n\pi z), \tag{3.2}$$

$$\hat{w}^{m,n} = -\sqrt{2}\cos(m\pi y/2)\sin(n\pi z). \tag{3.3}$$

https://doi.org/10.1017/jfm.2018.451 Published online by Cambridge University Press

The velocity can be recovered by

$$v(y, z, t) = \sum_{m,n} A_y^{m,n}(t)\hat{v}^{m,n}, \tag{3.4}$$

$$w(y, z, t) = \sum_{m,n} A_z^{m,n}(t)\hat{w}^{m,n}. \tag{3.5}$$

The projection is done componentwise by a scalar product in the L_2-space. The corresponding time series $A_y^{m,n}(t)$ and $A_z^{m,n}(t)$ can be obtained by

$$A_y^{m,n}(t) = \int_0^{y_{max}} \int_0^{z_{max}} v(y, z, t)\hat{v}^{m,n}\,\mathrm{d}y\,\mathrm{d}z, \tag{3.6}$$

$$A_z^{m,n}(t) = \int_0^{y_{max}} \int_0^{z_{max}} w(y, z, t)\hat{w}^{m,n}\,\mathrm{d}y\,\mathrm{d}z. \tag{3.7}$$

A value $M^{m,n}(t)$ representing the contribution of different modes can be evaluated by $M^{m,n}(t) = \sqrt{A_y^{m,n}(t)^2 + A_z^{m,n}(t)^2}$. The mode (m, n) corresponds to a flow structure with m rolls in the y direction and n rolls in the z direction. Although Fourier basis functions do not satisfy the no-slip boundary conditions, it has been shown that they capture the convective flow profiles well (Chandra & Verma 2011, 2013; Petschel *et al.* 2011; Verma *et al.* 2015). The Fourier mode decomposition method has been employed extensively to study 2D reversals (Chandra & Verma 2011, 2013; Petschel *et al.* 2011; Verma *et al.* 2015) and heat transfer in quasi-2D cells (Wagner & Shishkina 2013; Chong *et al.* 2018).

We quantitatively analyse the flow mode competition for a representative case with $Ra = 10^7$, $Pr = 0.5$ and $\Gamma = 2$ where flow reversals only happen in a limited β range, i.e. $7^\circ \leqslant \beta \leqslant 13^\circ$. Figure 9 shows the time evolution of the amplitudes of dominated modes (2, 1) and (1, 1), and the vertical velocity at the centre of the cell w_c for $\beta = 8^\circ$. A sign change of w_c can nicely indicate a reversal. The flow near the times $t = 890$ and 2110, which are denoted by vertical dash-dotted lines, can be viewed as cessations in a $\Gamma = 2$ cell. The growth of corner rolls does not trigger successful reversals near these two moments. In figure 9, it is found that the transient $M^{2,1}(t)$ approaches zero during reversals, while $M^{1,1}(t)$ shows a spike. The vanishing of the (2, 1) mode and the appearance of the (1, 1) mode correspond to the appearance of the anticlockwise single-roll structures during the reversal. So we conclude that the appearance of single-roll mode (1, 1) plays a critical role in triggering a reversal, similar to that in a $\Gamma = 1$ cell where the (2, 2) mode plays the dominant role.

To understand why the flow reversals occur in a limited range of β, the bifurcation diagram is further shown in figure 10. One sees that the flow is dominated by the (2, 1) mode for $0^\circ \leqslant \beta \leqslant 6^\circ$ and the amplitude of the (1, 1) mode approaches 0, which is referred to as regime I. The $M^{1,1}$ starts to grow rapidly beyond $\beta = 7^\circ$, then flow reversals occur for $7^\circ \leqslant \beta \leqslant 13^\circ$, and we call this regime II. In this regime, the flow is still dominated by the (2, 1) mode, but the $M^{2,1}$ and $M^{1,1}$ are comparable. For $15^\circ \leqslant \beta \leqslant 90^\circ$, the flow is dominated by the (1, 1) mode and the amplitude of the (2, 1) mode is close to 0, which is called regime III. It can be seen that the $M^{1,1}$ decreases monotonically with increasing β in this regime; this is because the flow strength, which is denoted by the Reynolds number Re, decreases monotonically with increasing β in this regime (Guo *et al.* 2015; Shishkina & Horn 2016). It is clear that the reversals tend to happen in the intermediate β range where the (2, 1) mode and (1, 1) mode have comparable strengths. Based on the mode decomposition analysis, we conclude that the flow reversals in tilted cells for $\Gamma = 2$ can be viewed as a mode competition process between the (2, 1) mode and (1, 1) mode.

https://doi.org/10.1017/jfm.2018.451 Published online by Cambridge University Press

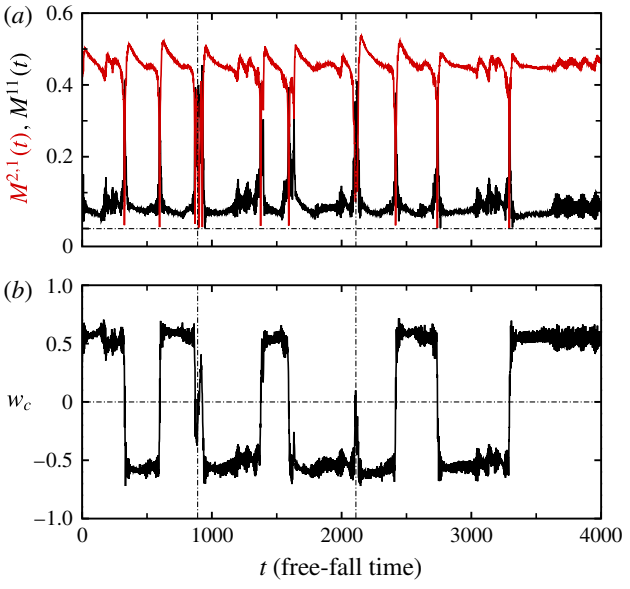


FIGURE 9. (Colour online) For $Ra = 10^7$, $Pr = 0.5$ and $\beta = 8°$, the time evolution of (a) flow mode amplitude of $M^{2,1}(t)$ (red line) and $M^{1,1}(t)$ (black line); and (b) vertical velocity component w_c at the centre location (1, 0.5).

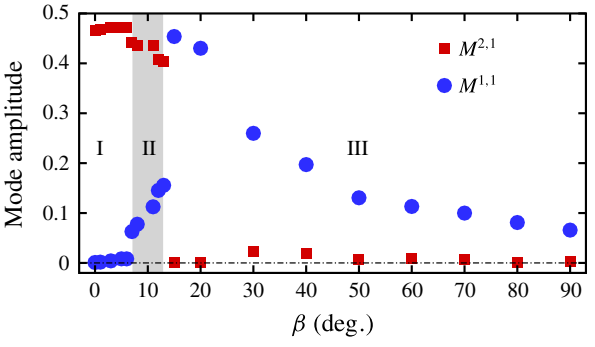


FIGURE 10. (Colour online) Time-averaged flow mode amplitudes $M^{1,1}$ and $M^{2,1}$ as a function of β for $Ra = 10^7$, $Pr = 0.5$ and $\Gamma = 2$; the grey area denotes the angle at which flow reversals appear.

3.3. *Heat transfer during flow reversals*

Finally, we discuss the heat transfer properties during a flow reversal. It is well recognized that heat transfer is closely connected to the mean flow structures in both two dimensions (van der Poel *et al.* 2011) and three dimensions (Sun *et al.* 2005; Xi & Xia 2008*b*; Bailon-Cuba, Emran & Schumacher 2010; Weiss & Ahlers 2011; Xia 2011; Huang *et al.* 2013; Chong *et al.* 2015). As shown above, during a flow reversal, the flow structures change greatly, so a significant change of heat transfer is

https://doi.org/10.1017/jfm.2018.451 Published online by Cambridge University Press

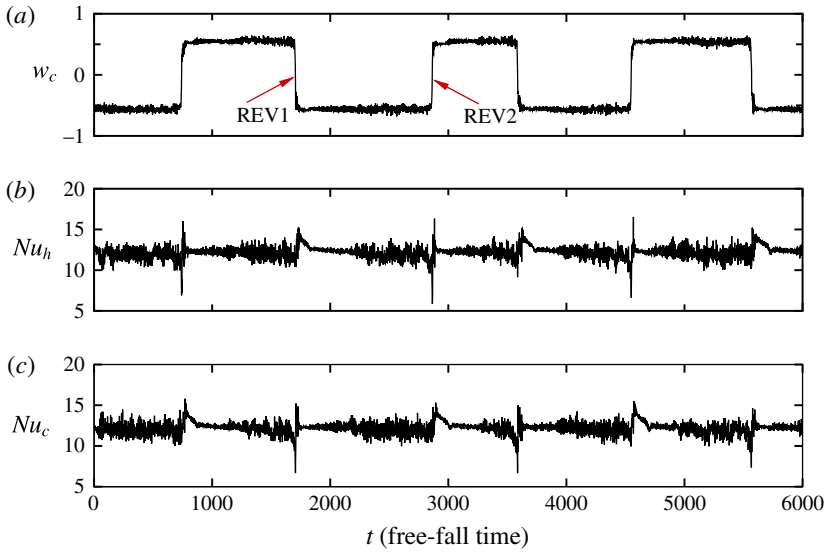


FIGURE 11. (Colour online) Time evolution of (*a*) vertical velocity at the cell centre w_c, (*b*) Nusselt number at the hot wall Nu_h, and (*c*) Nusselt number at the cold wall Nu_c, for $Ra = 10^7$, $Pr = 0.71$ and $\beta = 1^\circ$.

expected. The Nusselt number (Nu), used to measure heat transport, is defined as

$$Nu(t) = \frac{\hat{Q}}{\hat{k}\Delta\hat{T}/\hat{H}} = \frac{(\langle\hat{\rho}\hat{c}_p\hat{w}\hat{T}\rangle_A + \langle\hat{k}\partial_z\hat{T}\rangle_A)}{\hat{k}\Delta\hat{T}/\hat{H}}, \tag{3.8}$$

where $\hat{Q}$ is the heat flux across any horizontal plane (3D) or line (2D), and $\langle\cdot\rangle$ denotes averaging over any horizontal plane (3D) or line (2D). Here, Nu averaged over the hot and cold plate are denoted as Nu_h and Nu_c, respectively.

Figure 11 shows the time evolution of the vertical velocity component at the cell centre w_c, Nu_h and Nu_c for $Ra = 10^7$, $Pr = 0.71$, $\Gamma = 2$ and $\beta = 1^\circ$. We distinguish the two kinds of reversals by the sign change of w_c, referred to as REV1 and REV2. For REV1, Nu_h experiences a minor decrease, and then an overshoot; after a relatively long time, it returns to its normal value; Nu_c has a drastic decrease during the reversal; after an overshoot, it returns to its normal value quickly. For REV2, the behaviour of Nu_h is similar to that of Nu_c in REV1 and Nu_c is similar to that of Nu_h in REV1. These phenomena are similar to that in a level case. The most significant feature for $\Gamma = 2$ is that Nu_h and Nu_c behave differently during a reversal.

To better illustrate this point, the time evolutions of ensemble-averaged Nu_h and Nu_c are shown in figure 12. For $\Gamma = 2$, we first locate the data point where w_c becomes zero corresponding to the appearance of a single-roll mode during reversals. Then starting from this data point we go forward and backward for 500 free-fall time units. We averaged over 59/62 samples for REV1/REV2, and the results are plotted in figure 12(*a*) and (*b*). Similar procedures were also used before (Castillo-Castellanos *et al.* 2016; Xi *et al.* 2016) and in the study of statistical properties of geomagnetic field reversals (Valet *et al.* 2012). One can see from figure 12(*a*) that both Nu_h and Nu_c drop to their minima at $t \approx 0$ corresponding to the appearance of a single-roll mode during REV1. The Nu_c has a more drastic decrease than Nu_h, due to

https://doi.org/10.1017/jfm.2018.451 Published online by Cambridge University Press

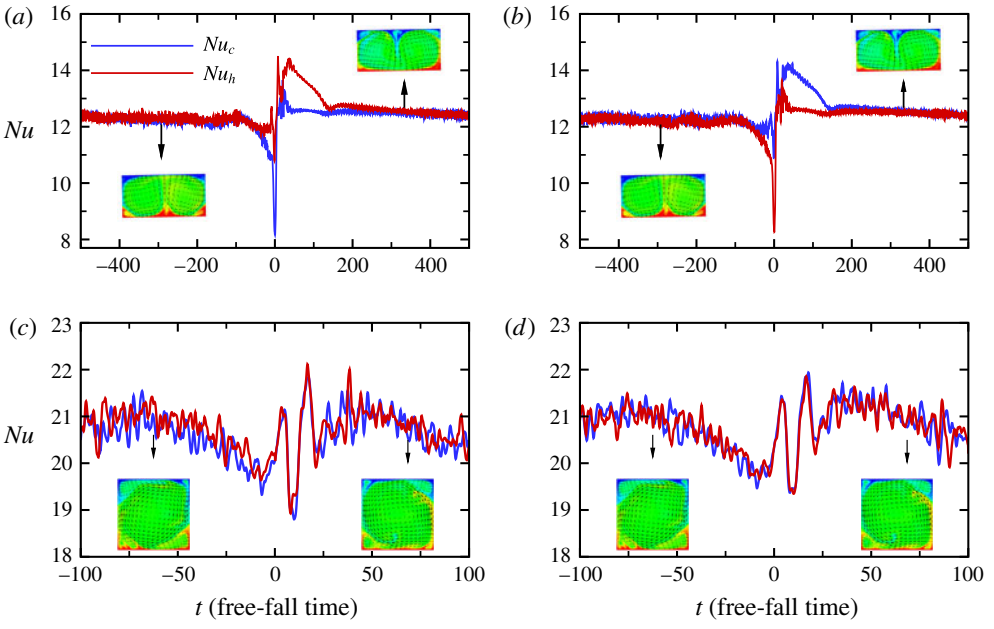


FIGURE 12. (Colour online) Time evolution of ensemble-averaged Nu_c and Nu_h during flow reversals for (*a*,*b*) $Ra = 10^7$, $Pr = 0.71$, $\beta = 1^\circ$ and $\Gamma = 2$ and (*c*,*d*) $Ra = 5 \times 10^7$, $Pr = 2$, $\beta = 0^\circ$ and $\Gamma = 1$. (*a*) REV1. (*b*) REV2. (*c*) The reversal from the clockwise single-roll mode to the anticlockwise single-roll mode. (*d*) The inverse process of (*c*).

apparent top-down asymmetric flow structures as shown in figure 5(*c*). There is also a small overshoot for Nu_h before reaching its local minimum. After reaching their local minima, both Nu_h and Nu_c increase rapidly. The Nu_c experiences some fluctuations around its local maximum, and then returns to its normal value. While for Nu_h, two local maxima are found, and it takes more time for Nu_h to return to its normal value. For REV2, the behaviours of Nu_h and Nu_c are reversed compared to REV1, as shown in figure 12(*b*). For comparison, Nu_h and Nu_c for $\Gamma = 1$ during two kinds of flow reversals are also plotted in figures 12(*c*) and 12(*d*). The time $t = 0$ is the time when the global angular momentum L becomes 0, corresponding to the appearance of the (2, 2) mode during the reversal, which is top-down symmetric. It is clear that Nu_h and Nu_c always have the same trend. It is interesting that the overshoot phenomenon is observed, which is similar to that in a cylindrical cell (Xi *et al.* 2016). In short, the heat transfer is directly connected with flow structures. The different trends of Nu_h and Nu_c during a reversal in a $\Gamma = 2$ cell are due to the preference for single corner roll growth during a reversal; while for $\Gamma = 1$, two corner rolls grow simultaneously, and the flow structure is symmetrical about the horizontal centreline, thus Nu_c and Nu_h behave the same.

4. Summary

In this work, we investigate the effect of cell tilt on flow reversals in $\Gamma = 1$ and 2 cells by performing 2D DNS. It is found that flow reversals are suppressed by tilt for $\Gamma = 1$. However, flow reversals characterized by two main rolls are greatly promoted by tilt for $\Gamma = 2$. For $\Gamma = 1$, flow reversals in tilted cells are led by the

https://doi.org/10.1017/jfm.2018.451 Published online by Cambridge University Press

simultaneous growth of two corner rolls, which is qualitatively the same as those in level cases. For $\Gamma = 2$, due to the introduction of a horizontal buoyancy force by tilt, flow reversals in a tilted cell are always led by the growth of the bottom-right or the top-left corner roll, which is different from those in a level case, where the four corner rolls all have opportunities to grow and trigger a reversal. Tilt is favourable for the thermal plumes to feed the bottom-right or the top-left corner roll, thus breaking the balance between the two main rolls and leading to a reversal. As a result, the reversals are promoted by tilt and are much more frequent than those in level cells. Moreover, flow reversals in tilted cells with $\Gamma = 2$ tend to occur for small Pr. Tilt broadens the Ra–Pr parameter space for flow reversals to happen in a $\Gamma = 2$ cell. Our study expands the flow reversals in a canonical system to small Pr, which is relevant to many geophysical and astrophysical flows (Schumacher, Götzfried & Scheel 2015; Scheel & Schumacher 2016). By exploiting the large-scale mode decomposition analysis, we demonstrate that flow reversals in a tilted cell with $\Gamma = 2$ can be viewed as a mode competition process between the single-roll mode and horizontally adjacent double-roll mode. Reversals can only occur in an intermediate range of β where $M^{1,1}$ and $M^{2,1}$ are comparable. Furthermore, we find that Nu_h and Nu_c behave the same during a reversal for $\Gamma = 1$, but they behave differently for $\Gamma = 2$ due to preference for single corner roll growth during a reversal.

The present finding of more frequent flow reversals in a tilted $\Gamma = 2$ cell demonstrates that the effects of symmetry breaking on flow reversals are system-dependent, which should still be explored in asymmetrical systems to gain more physical insights into the various reversal phenomena in nature.

Acknowledgements

This work is supported by the National Natural Science Foundation of China under grants 11572314, 11502137, 11772323 and 11621202, and by the Fundamental Research Funds for the Central Universities.

REFERENCES

AHLERS, G., GROSSMANN, S. & LOHSE, D. 2009 Heat transfer and large scale dynamics in turbulent Rayleigh–Bénard convection. *Rev. Mod. Phys.* **81**, 503–537.

ARAUJO, F. F., GROSSMANN, S. & LOHSE, D. 2005 Wind reversals in turbulent Rayleigh–Bénard convection. *Phys. Rev. Lett.* **95**, 084502.

BAILON-CUBA, J., EMRAN, M. S. & SCHUMACHER, J. 2010 Aspect ratio dependence of heat transfer and large-scale flow in turbulent convection. *J. Fluid Mech.* **655**, 152–173.

BAO, Y., CHEN, J., LIU, B.-F., SHE, Z.-S., ZHANG, J. & ZHOU, Q. 2015 Enhanced heat transport in partitioned thermal convection. *J. Fluid Mech.* **784**, R5.

BENZI, R. 2005 Flow reversal in a simple dynamical model of turbulence. *Phys. Rev. Lett.* **95**, 024502.

BROWN, E. & AHLERS, G. 2006 Rotations and cessations of the large-scale circulation in turbulent Rayleigh–Bénard convection. *J. Fluid Mech.* **568**, 351–386.

BROWN, E. & AHLERS, G. 2007 Large-scale circulation model for turbulent Rayleigh–Bénard convection. *Phys. Rev. Lett.* **98**, 134501.

BROWN, E. & AHLERS, G. 2008 Azimuthal asymmetries of the large-scale circulation in turbulent Rayleigh–Bénard convection. *Phys. Fluids* **20**, 105105.

BROWN, E., NIKOLAENKO, A. & AHLERS, G. 2005 Reorientation of the large-scale circulation in turbulent Rayleigh–Bénard convection. *Phys. Rev. Lett.* **95**, 084503.

CASTILLO-CASTELLANOS, A., SERGENT, A. & ROSSI, M. 2016 Reversal cycle in square Rayleigh–Bénard cells in turbulent regime. *J. Fluid Mech.* **808**, 614–640.

https://doi.org/10.1017/jfm.2018.451 Published online by Cambridge University Press

CHANDRA, M. & VERMA, M. K. 2011 Dynamics and symmetries of flow reversals in turbulent convection. *Phys. Rev.* E **83**, 067303.

CHANDRA, M. & VERMA, M. K. 2013 Flow reversals in turbulent convection via vortex reconnections. *Phys. Rev. Lett.* **110**, 114503.

CHONG, K.-L., HUANG, S.-D., KACZOROWSKI, M. & XIA, K.-Q. 2015 Condensation of coherent structures in turbulent flows. *Phys. Rev. Lett.* **115**, 264503.

CHONG, K.-L., WAGNER, S., KACZOROWSKI, M., SHISHKINA, O. & XIA, K.-Q. 2018 Effect of Prandtl number on heat transport enhancement in Rayleigh–Bénard convection under geometrical confinement. *Phys. Rev. Fluid* **3** (1), 013501.

VAN DOORN, E., DHRUVA, B., SREENIVASAN, K. R. & CASSELLA, V. 2000 Statistics of wind direction and its increments. *Phys. Fluids* **12**, 1529–1534.

FOROOZANI, N., NIEMELA, J. J., ARMENIO, V. & SREENIVASAN, K. R. 2017 Reorientations of the large-scale flow in turbulent convection in a cube. *Phys. Rev.* E **95**, 033107.

GLATZMAIER, G. A., COE, R. S., HONGRE, L. & ROBERTS, P. H. 1999 The role of the Earth's mantle in controlling the frequency of geomagnetic reversals. *Nature* **401**, 885–890.

GLATZMAIER, G. A. & ROBERTS, P. H. 1995 A three-dimensional self-consistent computer simulation of a geomagnetic field reversal. *Nature* **377**, 203–209.

GUBBINS, D., SREENIVASAN, B., MOUND, J. & ROST, S. 2011 Melting of the Earth's inner core. *Nature* **473**, 361–363.

GUO, S.-X., ZHOU, S.-Q., CEN, X.-R., QU, L., LU, Y.-Z., SUN, L. & SHANG, X.-D. 2015 The effect of cell tilting on turbulent thermal convection in a rectangular cell. *J. Fluid Mech.* **762**, 273–287.

GUO, S.-X., ZHOU, S.-Q., QU, L., LU, Y.-Z., SUN, L. & SHANG, X.-D. 2017 Evolution and statistics of thermal plumes in tilted turbulent convection. *Intl J. Heat Mass Transfer* **111**, 933–942.

HOWARD, R. & LABONTE, B.-J. 1980 The Sun is observed to be a torsional oscillator with a period of 11 years. *Astrophys. J.* **239**, L33–L36.

HUANG, S.-D., KACZOROWSKI, M., NI, R. & XIA, K.-Q. 2013 Confinement-induced heat-transport enhancement in turbulent thermal convection. *Phys. Rev. Lett.* **111**, 104501.

HUANG, S.-D., WANG, F., XI, H.-D. & XIA, K.-Q. 2015 Comparative experimental study of fixed temperature and fixed heat flux boundary conditions in turbulent thermal convection. *Phys. Rev. Lett.* **115**, 154502.

HUANG, S.-D. & XIA, K.-Q. 2016 Effects of geometric confinement in quasi-2-D turbulent Rayleigh–Bénard convection. *J. Fluid Mech.* **794**, 639–654.

HUANG, Y.-X. & ZHOU, Q. 2013 Counter-gradient heat transport in two-dimensional turbulent Rayleigh–Bénard convection. *J. Fluid Mech.* **737**, R3.

MANNATTIL, M., PANDEY, A., VERMA, M. K. & CHAKRABORTY, S. 2017 On the applicability of low-dimensional models for convective flow reversals at extreme Prandtl numbers. *Eur. Phys. J.* B **90**, 259.

MISHRA, P. K., DE, A. K., VERMA, M. K. & ESWARAN, V. 2011 Dynamics of reorientations and reversals of large-scale flow in Rayleigh–Bénard convection. *J. Fluid Mech.* **668**, 480–499.

NI, R., HUANG, S.-D. & XIA, K.-Q. 2015 Reversals of the large-scale circulation in quasi-2D Rayleigh–Bénard convection. *J. Fluid Mech.* **778**, R5.

PETSCHEL, K., WILCZEK, M., BREUER, M., FRIEDRICH, R. & HANSEN, U. 2011 Statistical analysis of global wind dynamics in vigorous Rayleigh–Bénard convection. *Phys. Rev.* E **84**, 026309.

PODVIN, B. & SERGENT, A. 2015 A large-scale investigation of wind reversal in a square Rayleigh–Bénard cell. *J. Fluid Mech.* **766**, 172–201.

PODVIN, B. & SERGENT, A. 2017 Precursor for wind reversal in a square Rayleigh–Bénard cell. *Phys. Rev.* E **95**, 013112.

VAN DER POEL, E. P., OSTILLA-MÓNICO, R., VERZICCO, R., GROSSMANN, S. & LOHSE, D. 2015 Logarithmic mean temperature profiles and their connection to plume emissions in turbulent Rayleigh–Bénard convection. *Phys. Rev. Lett.* **115**, 154501.

https://doi.org/10.1017/jfm.2018.451 Published online by Cambridge University Press

VAN DER POEL, E. P., OSTILLA-MÓNICO, R., VERZICCO, R. & LOHSE, D. 2014 Effect of velocity boundary conditions on the heat transfer and flow topology in two-dimensional Rayleigh–Bénard convection. *Phys. Rev.* E **90**, 013017.

VAN DER POEL, E. P., STEVENS, R. J. A. M. & LOHSE, D. 2011 Connecting flow structures and heat flux in turbulent Rayleigh–Bénard convection. *Phys. Rev.* E **84**, 045303.

VAN DER POEL, E. P., STEVENS, R. J. A. M., SUGIYAMA, K. & LOHSE, D. 2012 Flow states in two-dimensional Rayleigh–Bénard convection as a function of aspect-ratio and Rayleigh number. *Phys. Fluids* **24**, 085104.

SCHEEL, J. D. & SCHUMACHER, J. 2016 Global and local statistics in turbulent convection at low Prandtl numbers. *J. Fluid Mech.* **802**, 147–173.

SCHUMACHER, J., GÖTZFRIED, P. & SCHEEL, J. D. 2015 Enhanced enstrophy generation for turbulent convection in low-Prandtl-number fluids. *Proc. Natl Acad. Sci. USA* **112**, 9530–9535.

SHISHKINA, O. & HORN, S. 2016 Thermal convection in inclined cylindrical containers. *J. Fluid Mech.* **790**, R3.

SHISHKINA, O. & WAGNER, C. 2011 Modelling the influence of wall roughness on heat transfer in thermal convection. *J. Fluid Mech.* **686**, 568–582.

SUGIYAMA, K., CALZAVARINI, E., GROSSMANN, S. & LOHSE, D. 2009 Flow organization in two-dimensional non-Oberbeck–Boussinesq Rayleigh–Bénard convection in water. *J. Fluid Mech.* **637**, 105–135.

SUGIYAMA, K., NI, R., STEVENS, R. J. A. M., CHAN, T.-S., ZHOU, S.-Q., XI, H.-D., SUN, C., GROSSMANN, S., XIA, K.-Q. & LOHSE, D. 2010 Flow reversals in thermally driven turbulence. *Phys. Rev. Lett.* **105**, 034503.

SUN, C., XI, H.-D. & XIA, K.-Q. 2005 Azimuthal symmetry, flow dynamics, and heat transport in turbulent thermal convection in a cylinder with an aspect ratio of 0.5. *Phys. Rev. Lett.* **95**, 074502.

TOPPALADODDI, S., SUCCI, S. & WETTLAUFER, J. S. 2017 Roughness as a route to the ultimate regime of thermal convection. *Phys. Rev. Lett.* **118**, 074503.

VALET, J. P., FOURNIER, A., COURTILLOT, V. & HERRERO-BERVERA, E. 2012 Dynamical similarity of geomagnetic field reversals. *Nature* **490**, 89–93.

VERMA, M. K., AMBHIRE, S. C. & PANDEY, A. 2015 Flow reversals in turbulent convection with free-slip walls. *Phys. Fluids* **27**, 047102.

VERMA, M. K., KUMAR, A. & PANDEY, A. 2017 Phenomenology of buoyancy-driven turbulence: recent results. *New J. Phys.* **19**, 025012.

WAGNER, S. & SHISHKINA, O. 2013 Aspect-ratio dependency of Rayleigh–Bénard convection in box-shaped containers. *Phys. Fluids* **25**, 085110.

WANG, Q., XU, B.-L., XIA, S.-N., WAN, Z.-H. & SUN, D.-J. 2017 Thermal convection in a tilted rectangular cell with aspect ratio 0.5. *Chin. Phys. Lett.* **34**, 104401.

WEISS, S. & AHLERS, G. 2011 Turbulent Rayleigh–Bénard convection in a cylindrical container with aspect ratio $\Gamma = 0.50$ and Prandtl number $Pr = 4.38$. *J. Fluid Mech.* **676**, 5–40.

XI, H.-D., LAM, S. & XIA, K.-Q. 2004 From laminar plumes to organized flows: the onset of large-scale circulation in turbulent thermal convection. *J. Fluid Mech.* **503**, 47–56.

XI, H.-D. & XIA, K.-Q. 2007 Cessations and reversals of the large-scale circulation in turbulent thermal convection. *Phys. Rev.* E **75**, 066307.

XI, H.-D. & XIA, K.-Q. 2008*a* Azimuthal motion, reorientation, cessation, and reversal of the large-scale circulation in turbulent thermal convection: a comparative study in aspect ratio one and one-half geometries. *Phys. Rev.* E **78**, 036326.

XI, H.-D. & XIA, K.-Q. 2008*b* Flow mode transitions in turbulent thermal convection. *Phys. Fluids* **20**, 055104.

XI, H.-D., ZHANG, Y.-B., HAO, J.-T. & XIA, K.-Q. 2016 Higher-order flow modes in turbulent Rayleigh–Bénard convection. *J. Fluid Mech.* **805**, 31–51.

XI, H.-D., ZHOU, Q. & XIA, K.-Q. 2006 Azimuthal motion of the mean wind in turbulent thermal convection. *Phys. Rev.* E **73**, 056312.

XIA, K.-Q. 2011 How heat transfer efficiencies in turbulent thermal convection depend on internal flow modes. *J. Fluid Mech.* **676**, 1–4.

https://doi.org/10.1017/jfm.2018.451 Published online by Cambridge University Press

XIA, K.-Q. 2013 Current trends and future directions in turbulent thermal convection. *Theor. Appl. Mech. Lett.* **3**.

XIA, S.-N., WAN, Z.-H., LIU, S., WANG, Q. & SUN, D.-J. 2016 Flow reversals in Rayleigh–Bénard convection with non-Oberbeck–Boussinesq effects. *J. Fluid Mech.* **798**, 628–642.

XIE, Y.-C., WEI, P. & XIA, K.-Q. 2013 Dynamics of the large-scale circulation in high-Prandtl-number turbulent thermal convection. *J. Fluid Mech.* **717**, 322–346.

XU, B.-L., WANG, Q., WAN, Z.-H., YAN, R. & SUN, D.-J. 2018 Heat transport enhancement and scaling law transition in two-dimensional Rayleigh–Bénard convection with rectangular-type roughness. *Intl J. Heat Mass Transfer.* **121**, 872–883.

ZHANG, Y., HUANG, Y.-X., JIANG, N., LIU, Y.-L., LU, Z.-M., QIU, X. & ZHOU, Q. 2017*a* Statistics of velocity and temperature fluctuations in two-dimensional Rayleigh–Bénard convection. *Phys. Rev.* E **96**, 023105.

ZHANG, Y.-Z., SUN, C., BAO, Y. & ZHOU, Q. 2018 How surface roughness reduces heat transport for small roughness heights in turbulent Rayleigh–Bénard convection. *J. Fluid Mech.* **836**.

ZHANG, Y., ZHOU, Q. & SUN, C. 2017*b* Statistics of kinetic and thermal energy dissipation rates in two-dimensional turbulent Rayleigh–Bénard convection. *J. Fluid Mech.* **814**, 165–184.

ZHOU, Q., STEVENS, R. J. A. M., SUGIYAMA, K., GROSSMANN, S., LOHSE, D. & XIA, K.-Q. 2010 Prandtl–Blasius temperature and velocity boundary-layer profiles in turbulent Rayleigh–Bénard convection. *J. Fluid Mech.* **664**, 297–312.

ZHOU, Q., SUGIYAMA, K., STEVENS, R. J. A. M., GROSSMANN, S., LOHSE, D. & XIA, K.-Q. 2011 Horizontal structures of velocity and temperature boundary layers in two-dimensional numerical turbulent Rayleigh–Bénard convection. *Phys. Fluids* **23**, 125104.

ZHU, X.-J., MATHAI, V., STEVENS, R. J. A. M., VERZICCO, R. & LOHSE, D. 2018 Transition to the ultimate regime in two-dimensional Rayleigh–Bénard convection. *Phys. Rev. Lett.* **120**, 144502.

ZHU, X.-J., STEVENS, R. J. A. M., VERZICCO, R. & LOHSE, D. 2017 Roughness-facilitated local 1/2 scaling does not imply the onset of the ultimate regime of thermal convection. *Phys. Rev. Lett.* **119**, 154501.

https://doi.org/10.1017/jfm.2018.451 Published online by Cambridge University Press